https://doi.org/10.5194/egusphere-2026-6403
Preprint. Discussion started: 10 November 2026
© Author(s) 2026. CC BY 4.0 License.

Source-dependent wet scavenging of char and soot at a regional background site of the Yangtze River Delta region, China

Changliu Wu[1,2,3], Fang Cao[1,2,3*], Feng Xie[1,2,3], Yuxian Zhang[1,2,3], Xiaoying Yang[1,2,3], Wenhuai Song[1,2,3], Mingyuan Yu[1,2,3], Qianli Ma[4], Yuan Dai[2,5], Xiaofang Jia[6], Sönke Szidat[7], and Yanlin Zhang[1,2,3]

[1]School of Ecology and Applied Meteorology, Nanjing University of Information Science and Technology, Nanjing 210044, China.

[2]Jiangsu Key Laboratory of Intelligent Atmospheric Environment Monitoring and Carbon-Pollution Co-control, Nanjing University of Information Science and Technology, Nanjing 210044, China.

[3]State Key Laboratory of Climate System Prediction and Risk Management, Nanjing University of Information Science and Technology, Nanjing 210044, China.

[4]Zhejiang Lin'an, Atmospheric Background, National Observation and Research Station, Hangzhou 311300, China.

[5]Yangzhou Environmental Monitoring Center, Department of Ecology and Environment of Jiangsu Province, Yangzhou 225009, China.

[6]Meteorological Observation Center, China Meteorological Administration, Beijing 100081, China.

[7]Oeschger Centre for Climate Change Research, University of Bern, Bern 3012, Switzerland.

[*]**Corresponding author:** Fang Cao (caofangle@163.com)

https://doi.org/10.5194/egusphere-2026-6403
Preprint. Discussion started: 10 November 2026
© Author(s) 2026. CC BY 4.0 License.

Abstract

Atmospheric black carbon (BC) consists of two subfractions, char and soot, formed through different combustion processes and possessing distinct physicochemical properties. Here, we investigated the sources, precipitation-driven removal, and attenuation-derived apparent light absorption of char and soot in $PM_{2.5}$ at a regional background site in the Yangtze River Delta region, China, using a positive matrix factorization model constrained by ^{14}C-Latin Hypercube Sampling estimates. Char dominated BC mass (77.5 ± 12.7%), with higher concentrations in winter and autumn, whereas soot exhibited the opposite seasonal pattern. Wintertime char was mainly contributed by biomass burning (42.0%) and coal combustion (34.2%), consistent with enhanced regional transport from northern China. Traffic-related sources, including gasoline/diesel combustion and road dust, dominated char in spring (40.8%) and summer (48.7%), while heavy-oil combustion dominated in autumn (42.8%), potentially reflecting coastal/marine shipping emission. Soot was largely fossil-derived, with coal combustion dominating in winter (74.9%) and traffic-related sources prevailing in other seasons (58.3-65.4%). Precipitation exhibited a distinct selective scavenging effect, removing char, particularly biomass-derived char, more efficiently and consequently reducing its absorption. By contrast, soot concentration remained statistically unchanged, whereas its apparent absorption and MAE increased with precipitation amount, which is potentially linked to humidity-related changes in particle mixing state. These results demonstrate that source- and subfraction-dependent wet scavenging alters BC composition and apparent absorption, with important implications for interpreting BC observations and improving model representations in remote background/receptor regions.

https://doi.org/10.5194/egusphere-2026-6403
Preprint. Discussion started: 10 November 2026
© Author(s) 2026. CC BY 4.0 License.



43 **Keywords:** black carbon, light absorption, radiocarbon, source apportionment, wet
44 deposition

https://doi.org/10.5194/egusphere-2026-6403
Preprint. Discussion started: 10 November 2026
© Author(s) 2026. CC BY 4.0 License.

1 Introduction

Atmospheric black carbon (BC) particles play a crucial role in climate change, serving as an effective short-lived climate forcer (Chen et al., 2013; Li et al., 2024; Lohmann et al., 2020; Réveillet et al., 2022; Zeng et al., 2024). The environmental impacts of black carbon remain considerably uncertain, in part attributable to its heterogeneity (Cai et al., 2023; Geng et al., 2024; Zhang et al., 2021b). BC generally refers to all thermally altered carbonaceous substances formed by the incomplete combustion of fossil fuels or biofuels under low-oxygen conditions (Blanco-Donado et al., 2022; Coppola et al., 2022; Fierce et al., 2016; Liu et al., 2017; Réveillet et al., 2022). However, numerous studies have shown that BC can be subdivided into two categories based on the Thermal-Optical Analysis: char and soot (Han et al., 2008; Han et al., 2009), which have distinct formation mechanisms. Char is mainly generated from the combustion of solid residues (e.g., residential heating and agricultural fires), forming porous and oxygen-rich particles with high organic carbon content (Cai et al., 2023; Geng et al., 2024; Han et al., 2018). In contrast, soot is considered to form from volatile compounds that recondense from the high-temperature gas phase, with a smaller particle size, characterized by compact and hydrophobic aggregates dominated by elemental carbon (Han et al., 2022; Lohmann et al., 2020; Zhang et al., 2021b). physicochemical properties, atmospheric lifetimes, and radiative efficiencies (Cai et al., 2023; Geng et al., 2024; Zhang et al., 2021b).

The differences in physicochemical properties, such as hydrophilicity, light absorption properties and atmospheric lifetimes, are associated with formation pathways and combustion

https://doi.org/10.5194/egusphere-2026-6403
Preprint. Discussion started: 10 November 2026
© Author(s) 2026. CC BY 4.0 License.

sources (Cai et al., 2023; Han et al., 2018; Han et al., 2022; Zhang et al., 2021b). For example, soot generally exhibits higher mass absorption efficiencies (MAE) than char from the same source, except for biomass burning (BB) emissions where char can be more light-absorbing (Yang et al., 2025; Yu et al., 2025). The aging process further changes the mass concentration and MAE of char and soot, resulting in discrepancies when estimating BC radiative effects (Yu et al., 2025; Yu et al., 2026). Therefore, separating and quantifying the sources of char and soot, along with elucidating their physicochemical properties, are essential for a comprehensive understanding of their environmental and climatic impacts (Blanco-Donado et al., 2022; Cai et al., 2023; Geng et al., 2024; Zhang et al., 2021b).

Wet deposition (i.e., precipitation) is the dominant atmospheric removal pathway of BC, accounting for 60~85% of total BC deposition (Huang et al., 2010; Réveillet et al., 2022; Sharma et al., 2013; Zhang et al., 2025a). Previously, numerous studies have similarly pointed out the source-dependent wet removal effect of BC, generally showing more efficient removal of BC emitted from BB (BC_{bb}) than fossil-fuel-derived BC (BC_{ff}). For instance, a substantially higher wet scavenging ratio was reported for BC_{bb} (0.45) than for BC_{ff} (0.13) in the Nanjing urban area (Yu et al., 2026). Furthermore, $^{14}C_{BC}$ measurements revealed higher BC_{bb} proportions in rainwater or snow than in aerosol samples over the remote Tibetan Plateau region (Li et al., 2025), Alert in Canada (Rodríguez et al., 2020), and the urban area of Switzerland (Szidat et al., 2006; Zhang et al., 2015b). These observations suggested a source-dependent selective scavenging effect of BC aerosols occurred across both remote and urban environments worldwide. Considering that BC_{bb} was mainly composed of char, while relatively high soot content was measured in BC_{ff} (Cai et al., 2023; Han et al., 2018), it is

https://doi.org/10.5194/egusphere-2026-6403
Preprint. Discussion started: 10 November 2026
© Author(s) 2026. CC BY 4.0 License.

crucial to clarify the effects of wet deposition on the content and light absorption properties of atmospheric form- and source-specific BC for assessing its radiative forcing.

Previous studies have shown that char to soot (char/soot) ratios are influenced by fuel types (biofuel vs. fossil fuel) and combustion conditions (e.g., flaming vs. smoldering), limiting their robustness as source diagnostic indicators and introducing considerable uncertainty in source apportionment (Chow et al., 2004; Han et al., 2007;Chen et al., 2007; Xie et al., 2026; Liu et al., 2024). The positive matrix factorization (PMF) model, when integrated with molecular and elemental chemical fingerprints, enables quantitative attribution of char and soot contributions from multiple sources (Liang et al., 2016; Zheng et al., 2017), but the approach remains susceptible to considerable subjectivity, especially in factor selection and profile interpretation (Feng et al., 2024; Liang et al., 2016). Radiocarbon (^{14}C) can accurately distinguish BC_{bb} and BC_{ff} (Cao et al., 2017; Huang et al., 2014; Zhang et al., 2021a; Zhang et al., 2010; Zhang et al., 2015c; Zhang et al., 2015d), but lacks the resolution to further separate different sources. Consequently, the ^{14}C-constrained PMF method can significantly improve the objectivity and accuracy of source apportionment (Wang et al., 2023; Yang et al., 2025; Zhang et al., 2022; Wang et al., 2017b; Zong et al., 2016). This approach is particularly effective for complex mixed-source aerosols, such as those typically observed at background or remote sites (Wu et al., 2025; Feng et al., 2024; Wang et al., 2026).

Background sites, characterized by limited local emissions, are ideal for evaluating the impact of anthropogenic emissions on atmospheric constituents via regional transport (Zhang

https://doi.org/10.5194/egusphere-2026-6403
Preprint. Discussion started: 10 November 2026
© Author(s) 2026. CC BY 4.0 License.

et al., 2015a; Zhang et al., 2012). Consequently, background/receptor-observations are widely employed to constrain BC emission inventories and evaluate model performance (Cheng et al., 2017; Liu et al., 2025b; Zhu et al., 2020). These sites are also well suited to investigating transport-related aging and wet scavenging removal of char and soot, as regional transport dominates while contributions from short-duration local emission events remain limited (Li et al., 2025). ^{14}C measurements, when combined with organic tracers and statistical uncertainty propagation, have been widely used to constrain fossil and non-fossil contributions to carbonaceous aerosols at regional background and receptor sites. In particular, the Latin Hypercube Sampling (LHS) method provides a practical framework for quantifying uncertainties in source-specific emission ratios and measured carbonaceous components (Gelencsér et al., 2007; Szidat et al., 2009; Yttri et al., 2024; Yttri et al., 2011), and has been applied in previous organic aerosols and BC source apportionment studies in Europe and China (Niu et al., 2013; Yu et al., 2023; Zhang et al., 2024; Zhang et al., 2015c; Zhao et al., 2022). This integrated framework of radiocarbon and tracers proves especially valuable at background and receptor sites, where aerosols are regionally mixed and source signatures become altered during transport. For instance, it was quantified that the modern carbon fraction of BC was approximately 73 ± 12% (61% ~ 88%) by the ^{14}C-LHS method during winter at five background sites of the China Meteorological Administration Atmosphere Watch Network (CAWNET; Zhang et al., 2024).

In this study, year-round $PM_{2.5}$ samples were collected at the Lin'an site, a key regional background site within the Yangtze River Delta (YRD) region, exhibiting a relatively high level of fossil-derived pollution by regional transport from anthropogenic sources (Zhang et

https://doi.org/10.5194/egusphere-2026-6403
Preprint. Discussion started: 10 November 2026
© Author(s) 2026. CC BY 4.0 License.

al., 2024). The concentration of char and soot, as well as their light absorption properties, were measured based on the thermal-optical method. Building on the established ^{14}C-LHS estimation framework, the source contributions of char and soot were accurately quantified using a PMF model constrained by ^{14}C-LHS estimates. The impact of precipitation on the concentrations and light absorption of char and soot was further discussed, aiming to clarify source-dependent selective removal of char and soot, and to provide valuable insights for environmental policy formulation and climate effect assessment.

2 Materials and Methods

2.1 Field Sampling

Lin'an regional atmospheric background monitoring station (30°17'N, 119°45'E, 138.6m ASL) was set up in the YRD region by CMA according to the World Meteorological Organization (WMO) guideline for regional Global Atmosphere Watch (GAW) Station. The sampling site is on the top of a hill with a relative height of about 100 m, surrounded by rolling hills covered by patches of pine and bamboo forest, far from urban areas, with minimal local pollution, which serves as a regional receptor for air masses from the YRD region. Aerosol samples were collected using medium-volume samplers (Qingdao Laoshan) in Lin'an from Dec. 2019 to Jan. 2020, Mar. to May 2020 and May to Aug. 2020 as well as Aug. to Nov. 2020, with a flow rate of 100 L·min^{-1} for 23 h. Finally, the number of valid samples collected was 27 in winter, 30 in spring, 37 in summer and 35 in autumn, respectively. The sampling method was described in detail elsewhere (Wu et al., 2025; Zhang et al., 2024).

https://doi.org/10.5194/egusphere-2026-6403
Preprint. Discussion started: 10 November 2026
© Author(s) 2026. CC BY 4.0 License.

2.2 Laboratory Analysis

2.2.1 BC, Char and Soot

BC (also called elemental carbon, i.e., EC) was analyzed with a DRI Model 2001 thermal/optical carbon analyzer (Atmoslytic Inc., Calabasas, CA) following the IMPROVE_A thermal-optical reflectance (TOR) program. The temperature protocol was 140, 280, 480, and 580 °C in pure helium, producing four organic carbon (OC) fractions (OC_1 ~ OC_4, respectively) and a pyrolyzed carbon fraction (POC, determined when transmitted or reflected laser light reached its original intensity after oxygen was added to the analysis atmosphere). Then the filter was heated under an oxygen/helium atmosphere for three EC fractions (EC_1 ~ EC_3 at 580, 740, and 840 °C, respectively). The total BC is calculated as $EC_1 + EC_2 + EC_3 - POC$. Char is defined as EC_1 minus POC (char = $EC_1 - POC$), and soot is defined as the sum of EC_2 and EC_3 (soot = $EC_2 + EC_3$), according to Han et al. (2007 and 2018) and Zhi et al. (2011).

2.2.2 Other Chemical Analysis

To provide a comprehensive source apportionment of BC, we also measured the concentrations of organic molecular markers (including *n*-alkanes, polycyclic aromatic hydrocarbons (PAHs), hopanes, galactosan (GA), mannosan (MN), levoglucosan (LG)), water-soluble inorganic ions (Na^+, NH_4^+, K^+, Mg^{2+}, Ca^{2+}, Cl^-, NO_3^- and SO_4^{2-}), along with total metal and metalloid elements (V, Cr, Mn, Ni, Cu, Zn, Pb, Cd, Ba and As). The detection methods for organic molecular markers (Cao et al., 2021; Cao et al., 2024), water-soluble inorganic ions (Fan et al., 2020; Lin et al., 2022), along with total metal and metalloid

https://doi.org/10.5194/egusphere-2026-6403
Preprint. Discussion started: 10 November 2026
© Author(s) 2026. CC BY 4.0 License.

elements (Yang et al., 2025) were described previously. The ^{14}C measurement of total carbon (TC) in $PM_{2.5}$ samples was conducted using an OC/EC analyzer (Model 5L, Sunset Laboratory, USA) coupled with the accelerator mass spectrometer (AMS) system Mini Carbon Dating System (MICADAS) in the Laboratory for the Analysis of Radiocarbon (LARA), University of Bern, Switzerland, described previously for methodological details (Szidat et al., 2014; Wu et al., 2025). And details of the analytical procedure for all chemical tracers and ^{14}C of TC above were shown in the Text S1 of the Supporting Information.

2.2.3 Quality Assurance and Quality Control (QA/QC)

The QA/QC procedure for laboratory analysis mainly includes blank correction, parallel experiment and recovery correction. The environmental blank samples were collected before and after sampling, and treated in the same way as the actual samples. The detected concentration of the blank samples was less than 20% of the average detected concentration of the samples. Parallel samples are inserted in the sample testing process, that is, repeated analysis of some samples (standard deviation less than 15%) to ensure the repeatability and accuracy of the test. A standard sample of at least 5 gradients was prepared and tested before the experiment to obtain a standard curve with a correlation of at least 0.999. A suitable standard is selected for the same treatment as the actual sample to detect the recovery rate of the testing process, which is between 80% and 120% for all species. The details are described previously (Wu et al., 2025; Yang et al., 2025; Zhang et al., 2024).

2.3 Source Apportionment Methodologies

As shown in Figure S1, the LHS methodology was applied to quantitatively estimate the

https://doi.org/10.5194/egusphere-2026-6403
Preprint. Discussion started: 10 November 2026
© Author(s) 2026. CC BY 4.0 License.

relative contributions of fossil and non-fossil sources to BC in this study, using the data set from measured mass concentrations of OC, EC and LG, estimated emission ratios, and ^{14}C content of total aerosol carbon (Wu et al., 2025; Yang et al., 2025; Zhang et al., 2024). Briefly, the BC_{bb} concentrations were determined by the LG concentrations and the emission ratios of $(LG/OC)_{bb}$ and $(EC/OC)_{bb}$, and the BC_{ff} concentrations were calculated by subtracting BC_{bb} from BC. The modern carbon fractions of BC ($F_m{}^{14}C_{BC}$) were the ratios of BC_{bb} to BC. Details were presented in Text S2, Tables S1-S2 and Figures S2-S6 of the Supporting Information. Subsequently, the concentrations of BC_{bb} and BC_{ff} estimated by the LHS method and the multiple chemical species measured were input to the EPA PMF 5.0 model, including organic molecular markers, water-soluble ions, and metal elements. The concentrations of BC and char were set as the total variable, and the concentrations and contributions of soot from various sources were calculated based on mass conservation, i.e., $BC_i = char_i + soot_i$, and *i* represents the source here. Details were presented in Text S3, Tables S3-S5 and Figures S7-S8 of the Supporting Information.

The Lin'an sampling site was specified as the receptor, with an arrival height of 500 m above ground level. The NOAA HYSPLIT model was used to calculate 48h-backward trajectories for four synoptic arrival times (00:00, 06:00, 12:00, and 18:00 UTC). The resulting trajectories were clustered to characterize short- and long-range transport pathways, and infer the likely geographic source regions of air masses arriving at the site.

2.4 Calculation and Simulation of Mass Absorption Efficiency

According to the method in Ram and Sarin (2009), the abundance of EC and the

https://doi.org/10.5194/egusphere-2026-6403
Preprint. Discussion started: 10 November 2026
© Author(s) 2026. CC BY 4.0 License.

absorption coefficient could be estimated simultaneously based on the optical attenuation feature in the thermo-optical carbon analyzer. And (Ammerlaan et al., 2017) further provided a detailed technical description of carbon analyzer as an absorption photometer, and used a multi-angle absorption photometer to calibrate the transmission-derived absorption of the carbon analyzer, revealing a precision of absorption coefficient and MAE for approximately 10%~12%. The light absorption coefficients at λ = 633 nm (*Abs*) of BC and its subfractions were measured in accordance with the transmitted signal intensities of carbon analyzer at different analysis stages as described in Section 2.2.1. The equations were as follows:

$$Abs = \frac{b_{ATN}}{C \cdot R(ATN)} = \frac{ATN \cdot A}{V \cdot C \cdot R(ATN)} \quad (1)$$

$$ATN = ln\left(\frac{I_0}{I}\right) \quad (2)$$

$$R(ATN) = \left(\frac{1}{f}\text{-}1\right)\left(\frac{ln(ATN)\text{-}\,ln\,(10)}{ln\,(50)\text{-}\,ln\,(10)}\right)+1 \quad (3)$$

where I_0 and I are the intensity of transmittance light signal measured before and end of the analysis, A (mm^2) is the filter area, V (m^3) is the sample volume, C and $R(ATN)$ are empirical correction factors used to account for artifacts caused by multiple scattering and shadowing effects (Ram and Sarin, 2009; Zhang et al., 2021b). The parameters of C and f were adopted with 2.14 and 1.1, respectively, as detailed in the previous studies (Liu et al., 2025a; Song et al., 2026; Xu et al., 2025; Yu et al., 2025). Subsequently, the MAE (λ = 633 nm) values of BC and its subfractions were calculated by the ratios of the b_{abs} to their atmospheric concentrations. And the MAE were apportioned to different emission sources as follows:

$$MAE_{BC} \cdot BC = \sum (MAE_{BC_i} \cdot BC_i) \quad (4)$$

https://doi.org/10.5194/egusphere-2026-6403
Preprint. Discussion started: 10 November 2026
© Author(s) 2026. CC BY 4.0 License.

$$MAE_{Char} \cdot Char = \sum (MAE_{Char_i} \cdot Char_i) \quad (5)$$

$$MAE_{Soot} \cdot Soot = \sum (MAE_{Soot_i} \cdot Soot_i) \quad (6)$$

where i represents the emission source.

Data preliminary analysis and multiple linear regression (MLR) calculation were conducted with Microsoft Excel and Origin 2026, aiming to quantify the MAE of different emission sources or subfractions (i.e., char and soot) over Lin'an. The MAE of each component and the proportion of emission sources obtained based on ^{14}C-LHS-PMF were input into the software system to conduct regression analysis. Finally, the absorption characteristics of different BC subfractions from different sources were revealed.

Notably, Bond and Bergstrom (2006) further pointed out that the MAE of fresh light-absorbing carbon at a wavelength of 550 nm is approximately 7.5 ± 1.2 $m^2 \cdot gC^{-1}$, and the coating and mixed state can significantly affect its absorption. Collaud-Coen et al. (2010) systematically explored issues such as filter-loading amount, shadowing/multiple scattering and their correction in the filter-based absorption. And Drinovec et al. (2017) explained that the filter-loading effect is influenced by filter material, equipment, particle type, coating, and aging factors. Overall, the attenuation-based absorption estimates could be affected by multiple scattering, shadowing, filter-loading effects, filter matrix, and particle mixing state. Thus, the reported MAE values should be interpreted as the apparent MAE, and used mainly for relative comparisons rather than as absolute replacements for actual absorption measurements.

https://doi.org/10.5194/egusphere-2026-6403
Preprint. Discussion started: 10 November 2026
© Author(s) 2026. CC BY 4.0 License.

In this study, the apparent MAE served as a quantitative metric mainly to assess relative differences among various BC subfractions, emission sources, and precipitation patterns under a consistent analytical protocol. And the sensitivity tests varying the empirical correction parameters and excluding high-loading samples consistently reproduced the observed relative differences between char and soot or between rainy and non-rainy days (discussed in Section 3.3 for details), demonstrating the robustness of the observed relative patterns, as further elaborated in Text S4, Tables S6-S8 and Figure S9 of the Supporting Information.

3 Results and Discussion

3.1 Temporal variations of BC, char, and soot.

The time series of mass concentrations for BC, char, and soot in $PM_{2.5}$ over Lin'an during the observation period, are presented in Figure 1 and Table S9. The annual mean BC concentration was 2.4 ± 1.1 $\mu gC \cdot m^{-3}$ (range: 0.8 ~ 6.7 $\mu gC \cdot m^{-3}$), which was comparable to that reported at Chongming island (Xing, 2022), a coastal background receptor in the YRD region, and higher than those observed at other background sites in China, such as Wuyi Mountain (Ren et al., 2019), Beihuangcheng Island (Zong et al., 2018), but substantially lower than concentrations measured at Lin'an during 2014-2016 and at urban sites in the YRD region (Table S10). These comparisons suggested that BC concentrations in the YRD region have declined over the past few years, although levels remain higher than many other regions in China.

Char dominated the BC mass concentration, accounting for 77.5 ± 12.7 % (range: 46.8 ~

https://doi.org/10.5194/egusphere-2026-6403
Preprint. Discussion started: 10 November 2026
© Author(s) 2026. CC BY 4.0 License.

96.8 %), with an annual mean concentration of 2.0 ± 1.2 μgC·m^{-3} (range: 0.4 ~ 6.4 μgC·m^{-3}), lower than those observed in urban areas of the YRD region (Table S10). Char exhibited pronounced seasonal variability, with higher concentrations in autumn and winter and lower concentrations in spring and summer (Figure 1), consistent with observations at nearby urban sites (Han et al., 2010; Han et al., 2009). By contrast, soot concentrations were highest in summer (0.6 ± 0.2 μgC·m^{-3}), followed by spring (0.5 ± 0.2 μgC·m^{-3}), winter (0.4 ± 0.1 μgC·m^{-3}), and autumn (0.3 ± 0.1 μgC·m^{-3}). The contrasting seasonal patterns of char and soot likely reflected differences in their sources, transport pathways, and removal processes. Weak correlations between their concentrations during most periods suggested partly distinct source and atmospheric processing (Figure S10). The concentration-weighted trajectory analyses identified inland provinces, including Anhui and Jiangxi, as potential source regions for char, whereas elevated soot was more frequently associated with trajectories passing over coastal urban and marine sectors (Figure S11). Furthermore, char may be removed more efficiently via wet deposition than soot (discussed in Section 3.3 for details), particularly during summer, when precipitation usually occurs more frequently the YRD region (Du et al., 2022; Liang et al., 2020), owing to its more hydrophilic property (Cai et al., 2026; Han et al., 2022).

3.2 Source apportionment of char and soot.

The char/soot ratios at Lin'an were compared with source-profile values reported for BB (13.2 ± 11.8), coal combustion (1.5 ± 0.4), and liquid fossil-fuel combustion (0.6 ± 0.2; Cao et al., 2007; Chen et al., 2007; Chow et al., 2004), as shown in Figure S13. The char/soot ratios varied markedly by season, with higher values in autumn (9.9 ± 6.2) and winter (8.6 ±

https://doi.org/10.5194/egusphere-2026-6403
Preprint. Discussion started: 10 November 2026
© Author(s) 2026. CC BY 4.0 License.

6.7) than in spring (4.0 ± 2.1) and summer (1.9 ± 0.7). The elevated char/soot ratios in the cold seasons suggest a stronger influence of BB and were supported by positive correlations between char/soot ratios and levoglucosan concentrations in winter and autumn (Figure S14). In contrast, the weak correlation in summer, together with the higher soot concentration, indicated a greater relative influence of non-BB sources, such as vehicular emissions. Because source-profile ratios can overlap and may change during atmospheric processing (Cai et al., 2023; Geng et al., 2024), these ratios are used here as qualitative rather than quantitative source indicators.

To quantify BC sources and investigate differences between the sources of char and soot, primary emission markers, including metal elements, water-soluble ions, combustion tracers (e.g., anhydrosugars, PAHs), and source fractions constrained by the ^{14}C-LHS analysis were integrated into a PMF model. A four-factor solution was finally selected as the optimal interpretation for Lin'an, as shown in Figure 2 and Figure S15. Factor 1 was assigned to BB sources, whereas factors 2 to 4 were interpreted as fossil-related sources on the basis of the PMF model results constrained by ^{14}C-LHS estimates. Factor 1 was characterized by high contributions of anhydrosugars and K^+, which are established tracers of BB emissions (Li et al., 2021; Wu et al., 2020; Zheng et al., 2021). Factor 2 was dominated by aromatic hydrocarbon markers associated with fossil fuel combustion (43.2~69.0%) (Cao et al., 2021), including fluoranthene (Fla, 48.2%), pyrene (Pyr, 54.9%), indeno (1,2,3-cd) pyrene (IcdP, 65.1%), benzo(ghi)perylene (BghiP, 60.4%), benzo(a)anthracene (BaA, 62.8%), chrysene (Chr, 51.9%), et al. The diagnostic ratios of those PAHs, such as Fla/(Fla+Pyr), IcdP/(IcdP+BghiP), and BaA/(BaA+Chr), were consistent with the endmembers of coal

https://doi.org/10.5194/egusphere-2026-6403
Preprint. Discussion started: 10 November 2026
© Author(s) 2026. CC BY 4.0 License.

combustion (Cao et al., 2021; Wu et al., 2020). Additionally, this factor also accounted for Pb (24.4%), Cd (21.1%), and As (16.2%), which are mainly derived from industrial emissions, including coal combustion (Lin et al., 2020). Therefore, factor 2 was assigned to coal combustion. Factor 3 was identified as a traffic-related mixture of exhaust emissions, non-exhaust emissions (e.g., brake/tire wear), and resuspension of road dust. It accounted for large fractions of Ca^{2+} (89.1%) and Mg^{2+} (76.3%), which are commonly associated with dust sources (Lin et al., 2020), as well as Ba (70.3%) and Cu (29.3%), which are tracers of non-exhaust traffic emissions (Yang et al., 2025). It exhibited relatively high loadings of liquid fossil fuel combustion tracers, such as V (35.0%), Cd (41.2%), phenanthrene (Phe, 34.3%) and anthracene (Ant, 45.7%), with a larger Ant/(Ant+Phe) ratio of > 0.1 (high-temperature combustion source; Cao et al., 2021; Lin et al., 2020; Wu et al., 2020). Annually, factor 3 accounted for 56.5% of soot, 26.0% of char, and 31.7% of BC. Factor 4 showed high contributions of V (39.0%), Ni (83.2%), Cr (54.4%), Mn (48.6%), Cu (40.8%), and Zn (70.8%), and revealed a pronounced seasonal pattern, with relatively high concentrations of V and Ni in summer (39.0% and 86.6%, respectively) and autumn (52.5% and 88.5%, respectively), consistent with heavy-oil combustion (Lin et al., 2020).

For annual mean contributions to total BC, traffic-related sources accounted for the largest contribution (31.7%), followed by heavy-oil combustion (27.2%), coal combustion (21.5%), and BB (19.6%). The source contributions differed substantially between char and soot. Char was mainly attributed to heavy-oil combustion (30.0%), traffic-related sources (26.0%), BB emissions (24.1%), and coal combustion (19.9%). Soot, by contrast, was dominated by traffic-related sources (56.5%), followed by coal combustion (28.4%) and

https://doi.org/10.5194/egusphere-2026-6403
Preprint. Discussion started: 10 November 2026
© Author(s) 2026. CC BY 4.0 License.

heavy-oil combustion (15.1%).

The contribution of traffic-related sources to char was higher in summer (48.7%) and spring (40.8%) than in autumn (20.1%) and winter (8.6%), potentially reflecting enhanced resuspension of road dust at higher temperatures and wind speeds. Notably, traffic-related sources contributed more than half of the soot in all seasons except winter, when coal combustion was the dominant source. The strong positive correlation between soot and Ca^{2+} (Figure S16), suggested an influence of non-exhaust vehicle emissions, such as road dust resuspension in soot. Heavy-oil combustion showed relatively high contributions in summer and autumn, coincided with a stronger influence of marine-sector air masses at Lin'an (Figure S12), and potential source regions over the Yellow Sea and East China Sea (Figure S17). These results suggested that shipping emission transported from coastal and marine areas may contributed to BC at the inland Lin'an background site.

Coal combustion showed higher contributions to BC in winter (39.0%), coincident with transport from northern source regions (Figure S17). It also accounted for a larger fraction of soot than of char across all seasons: winter (74.9% for soot vs. 34.2% for char), spring (21.5% vs. 17.0%), summer (12.6% vs. 10.6%), and autumn (28.6% vs. 13.1%). In contrast, biomass-derived BC was composed almost entirely of char, with higher contributions to total BC in winter (37.1%) and autumn (21.4%) than in spring (11.0%) and summer (3.4%), and BB was also the largest contributor to char (42.0%) in winter.

Overall, char, as the dominant BC subfraction, exhibited seasonal variations in source contributions similar to those of BC, whereas soot showed a contrasting seasonal pattern.

https://doi.org/10.5194/egusphere-2026-6403
Preprint. Discussion started: 10 November 2026
© Author(s) 2026. CC BY 4.0 License.

Solid fuel combustions, including biomass and coal, accounted for a larger fraction of char (44.0%) than soot (28.4%), particularly in winter. In contrast, traffic-related sources and heavy-oil combustion contributed more to soot (71.6%) than to char (56.0%), particularly in summer. Specifically, wintertime char was mainly contributed by BB (42.0%) and coal combustion (34.2%), attributing to enhanced regional transport from northern China. Traffic-related sources, including gasoline/diesel combustion and road dust, dominated char in spring (40.8%) and summer (48.7%), while heavy-oil combustion dominated in autumn (42.8%), potentially reflecting contributions from coastal and marine shipping emission. In contrast, soot was dominated by coal combustion in winter (74.9%) and traffic-related sources in other seasons (58.3-65.4%), with fossil-related sources accounting for nearly all soot at Lin'an.

3.3 Source-dependent wet scavenging of char and soot

Wet deposition plays an important yet poorly constrained role in regulating the atmospheric lifetime and optical properties of BC, with important implications for regional aerosol-climate interactions (Li et al., 2025). To investigate the effects of precipitation on different BC subfractions, samples collected throughout the observation period at Lin'an were classified into rainy days (daily precipitation > 0, N = 43) and non-rainy days (daily precipitation = 0, N = 86). A significantly stronger correlation was observed between atmospheric BC and carbon monoxide (CO) on non-rainy days (Pearson's $r = 0.68$, $p < 0.001$) compared to rainy days ($p > 0.05$) (Figure S18), indicating that precipitation strongly influenced BC concentrations. The atmospheric concentrations, apparent absorptions, and

https://doi.org/10.5194/egusphere-2026-6403
Preprint. Discussion started: 10 November 2026
© Author(s) 2026. CC BY 4.0 License.

apparent MAE values of char and soot were then statistically analyzed and calculated to evaluate the wet scavenging signatures of char and soot. Considering the empirical power-law dependence of aerosol wet removal on precipitation (Choi et al., 2020; Dasari et al., 2025), a log-log treatment using base-10 logarithms for correlation with precipitation amount was carried out.

As shown in Figure 3, the atmospheric concentration of char was significantly lower on rainy days than on non-rainy days ($p < 0.01$), with an average decrease of approximately 27%, indicative of efficient wet removal of char. In contrast, the soot concentration remained largely unaffected ($p > 0.05$), suggesting that soot was relatively persistent under rainy conditions. Consistent with this difference, char concentration was significantly and negatively correlated with precipitation amount on rainy days (Pearson's $r = -0.54$, $p < 0.001$), whereas no significant relationship was observed for soot ($p > 0.05$). These results collectively suggested a clear subfraction-dependent effect of precipitation on BC, with char being more efficiently scavenged than soot.

To explore the influence of precipitation on char and soot emitted from different sources, source-resolved concentrations obtained using the ^{14}C-LHS-PMF method were analyzed separately. As illustrated in Figure 4, pronounced source-dependent differences in the precipitation responses of BC subfractions were observed, particularly for char. The atmospheric concentration of biomass-derived char ($char_{bb}$) was significantly lower on rainy days than on non-rainy days ($p < 0.01$), with an average decrease of 49.9%, whereas fossil-fuel-derived char ($char_{ff}$) showed a smaller decrease of 16.7% that was not statistically

https://doi.org/10.5194/egusphere-2026-6403
Preprint. Discussion started: 10 November 2026
© Author(s) 2026. CC BY 4.0 License.

significant ($p \approx 0.06$). By contrast, the concentrations of fossil-fuel-derived soot ($soot_{ff}$), which accounted for nearly total soot in this study, showed no significant change ($p > 0.05$). On rainy days, $char_{bb}$ exhibited more significant negative relationship with precipitation amount (*slope* = -0.33, Pearson's r = -0.50, $p < 0.001$), compared with $char_{ff}$ (*slope* = -0.14, Pearson's r = -0.48, $p < 0.001$) and BC_{ff} (*slope* = -0.09, Pearson's r = -0.42, $p < 0.01$), while no significant relationship was observed for $soot_{ff}$ ($p > 0.05$). These results indicate that precipitation removed BC_{bb}, particularly its char component, more efficiently than BC_{ff}, especially $soot_{ff}$.

Collectively, these findings revealed a source- and subfraction-dependent wet scavenging efficiency of BC at Lin'an, driven by inter-source variations in the relative abundance and physicochemical properties of char and soot, which aligns with the previous observations of more efficient wet scavenging of BC_{bb} compared to BC_{ff} (Yu et al., 2026; Li et al., 2025; Rodríguez et al., 2020). Char, especially particles emitted from BB and residential coal combustion, commonly exhibit larger particle sizes, porous and structurally heterogeneous morphologies, and a greater abundance of oxygen-containing functional groups (Cai et al., 2026; Cai et al., 2023; Han et al., 2018; Han et al., 2022). These properties enhance their hydrophilicity and favor their incorporation into cloud droplets or their capture by precipitation. In contrast, soot particles, usually derived from liquid fossil fuel combustion and industrial coal combustion, exhibited relatively small size and more highly graphitized or aromatically condensed, resulting in greater hydrophobicity and lower wet scavenging efficiency.

https://doi.org/10.5194/egusphere-2026-6403
Preprint. Discussion started: 10 November 2026
© Author(s) 2026. CC BY 4.0 License.

3.4 Effects of wet scavenging on light absorption of char and soot.

The apparent MAE of char and soot also exhibited contrasting seasonal patterns, as shown in Figure 1(e). The apparent MAE_{char} was higher in autumn (10.1 ± 2.0 $m^2 \cdot gC^{-1}$) and winter (8.2 ± 1.4 $m^2 \cdot gC^{-1}$) than in spring (7.1 ± 1.9 $m^2 \cdot gC^{-1}$) and summer (5.4 ± 2.7 $m^2 \cdot gC^{-1}$). Conversely, the apparent MAE_{soot} was higher in summer (15.0 ± 2.4 $m^2 \cdot gC^{-1}$) and spring (12.7 ± 3.6 $m^2 \cdot gC^{-1}$) than in winter (10.1 ± 5.0 $m^2 \cdot gC^{-1}$) and autumn (8.8 ± 4.2 $m^2 \cdot gC^{-1}$). On an annual basis, soot exhibited a higher attenuation-derived apparent MAE (11.8 ± 4.5 $m^2 \cdot gC^{-1}$), compared to char (7.6 ± 2.7 $m^2 \cdot gC^{-1}$), indicating stronger light absorption properties. Similar differences have been reported during summer at the Mt. Hua alpine background site (MAE_{char}: 5.4 ± 2.5 $m^2 \cdot gC^{-1}$; MAE_{soot}: 13.7 ± 3.8 $m^2 \cdot gC^{-1}$) and during winter at several urban sites in northern China (MAE_{char}: 9.6 $m^2 \cdot gC^{-1}$; MAE_{soot}: 14.0 $m^2 \cdot gC^{-1}$; Liu et al., 2024; Liu et al., 2025a). In contrast, higher apparent MAE_{char} than MAE_{soot} was observed during a BB influenced winter haze episode at the rural Wangdu site (Xu et al., 2025) and during winter in Nanjing (Yu et al., 2025). These differences across sites and seasons may reflect variations in source composition, atmospheric processing, including changes in particle coating and mixing state (Cappa et al., 2012; Fu et al., 2021).

The contrasting effects of precipitation on the concentrations of char and soot were further reflected in their apparent light absorptions. Compared with non-rainy days, the apparent absorption of char decreased significantly by 33.7% on rainy days ($p < 0.01$), whereas the apparent absorption of soot increased significantly by 27.2% ($p < 0.01$). Correspondingly, apparent absorption of char was significantly and negatively correlated with

https://doi.org/10.5194/egusphere-2026-6403
Preprint. Discussion started: 10 November 2026
© Author(s) 2026. CC BY 4.0 License.

precipitation amount on rainy days (Pearson's r = -0.51, p < 0.001), whereas apparent absorption of soot exhibited a significant positive correlation (Pearson's r = 0.39, p < 0.05). Because the light absorption of each BC-subfraction is jointly determined by its atmospheric concentration and apparent MAE, these opposite responses indicated that rainy conditions affected the absorption of char and soot through different pathways.

To interpret these component-specific responses, the source apportionment results based on ^{14}C-LHS-PMF method were combined with attenuation-derived apparent MAE values using multiple linear regression (MLR). The robustness of this approach was evaluated through stability tests (Figure S19 and Figure S20) and statistical assessments (Tables S11-S13), supporting the reliability of the source-resolved apparent MAE estimates. As shown in Figure S21, BC_{bb} exhibited a lower apparent MAE (7.8 ± 0.5 $m^2 \cdot gC^{-1}$) than BC_{ff} (9.4 ± 0.2 $m^2 \cdot gC^{-1}$). These estimates were within the ranges reported by previous measurements and model-based assessments (BC_{ff}: 6.4 ~ 13.6 $m^2 \cdot gC^{-1}$; BC_{bb}: 1.8 ~ 19.7 $m^2 \cdot gC^{-1}$; Wu et al., 2021; Yan et al., 2019; Yu et al., 2025). Among the source-resolved BC components, $soot_{ff}$ exhibited the highest apparent MAE (13.5 ± 0.3 $m^2 \cdot gC^{-1}$), whereas the apparent MAE of $char_{bb}$ (8.1 ± 0.6 $m^2 \cdot gC^{-1}$) was slightly higher than that of $char_{ff}$ (7.4 ± 0.3 $m^2 \cdot gC^{-1}$). These results consistent with recent combustion-source measurements, which reported a higher apparent MAE for $char_{bb}$ (10.7 ± 9.3 $m^2 \cdot gC^{-1}$) than for $char_{ff}$ emitted from diesel vehicles (8.6 ± 4.3 $m^2 \cdot gC^{-1}$) and coal combustion (7.3 ± 2.9 $m^2 \cdot gC^{-1}$). In the same study, $soot_{ff}$ exhibited the strongest absorption among the investigated BC fractions, with apparent MAE of 12.4 ± 6.7 $m^2 \cdot gC^{-1}$ for diesel vehicle emissions and 12.2 ± 4.6 $m^2 \cdot gC^{-1}$ for coal combustion (Liu et al., 2025a).

https://doi.org/10.5194/egusphere-2026-6403
Preprint. Discussion started: 10 November 2026
© Author(s) 2026. CC BY 4.0 License.

These source-resolved differences provide a plausible explanation for the response of char absorption to precipitation. The apparent MAE_{char} did not differ significantly between rainy and non-rainy days ($p > 0.05$) and showed only a weak negative correlation with precipitation amount on rainy days (Pearson's r = -0.31, $p < 0.05$). Because $char_{bb}$ concentrations decreased more strongly on rainy days and $char_{bb}$ exhibited a slightly higher apparent MAE than $char_{ff}$, the relative contribution of $char_{bb}$ to the residual atmospheric char may have decreased under rainy conditions. This compositional shift would tend to reduce the apparent MAE of residual char particles, and may have offset the absorption enhancement associated with humidity-related coating growth or changes in particle mixing state (Figure S22). Consequently, the apparent MAE_{char} remained statistically unchanged and even decreased slightly with increasing precipitation amount. Given the substantial decrease in char concentration and the absence of an increase in the apparent MAE_{char}, the 33.7% reduction in apparent absorption of char was mainly driven by the efficient removal of char mass, particularly $char_{bb}$.

In contrast, the mass-specific absorption of soot exhibited a markedly different response. As shown in Figures 3(f) and 3(i), the apparent MAE_{soot} was, on average, 33.1% higher on rainy days than on non-rainy days, and was significantly and positively correlated with precipitation amount (Pearson's r = 0.46, $p < 0.001$). Because the soot concentrations remained statistically unchanged, the 27.2% increase in apparent absorption of soot was mainly attributable to the enhanced apparent MAE of the residual soot particles. This enhancement may have resulted from changes in particle mixing state and the hygroscopic growth of soot coatings under the high-humidity conditions prevalent during rainy periods.

https://doi.org/10.5194/egusphere-2026-6403
Preprint. Discussion started: 10 November 2026
© Author(s) 2026. CC BY 4.0 License.

As reported, the coatings of non-absorbing or weakly absorbing species, including sulfate, nitrate, and organic compounds, can increase BC absorption through the lensing effect, whereby the coating focuses incident radiation onto the absorbing BC core (Zhang et al., 2018; Zhang et al., 2025b; Wang et al., 2017a). Elevated ambient humidity, prevalent during rainy periods, facilitates the hygroscopic growth of these coatings, particularly the fossil-derived particles (Yu et al., 2026). Coincidentally, the significant positive correlations between the apparent MAE values of soot and ambient relative humidity were found in all seasons (Figure S22).

Precipitation was associated with contrasting changes in the apparent light absorption of char and soot through distinct pathways. For char, particularly $char_{bb}$, efficient wet scavenging reduced its atmospheric mass concentration and consequently decreased apparent light absorption. The preferential removal of the relatively high-MAE $char_{bb}$ fraction may also have prevented an increase in the apparent MAE of the residual char population. In contrast, soot was less efficiently scavenged, and its concentration remained relatively stable, whereas the apparent MAE of the residual soot particles increased under rainy and humid conditions, potentially attributed to hygroscopic coating growth and the associated lensing effect. Thus, the contrasting optical responses of char and soot arose from the combined effects of component-selective mass removal, source-composition changes, and humidity-related absorption enhancement.

4. Conclusions and Implications

In summary, char was the dominant BC subfraction in $PM_{2.5}$ at the regional background

https://doi.org/10.5194/egusphere-2026-6403
Preprint. Discussion started: 10 November 2026
© Author(s) 2026. CC BY 4.0 License.

site in the YRD, with higher concentrations in winter/autumn and lower concentrations in summer/spring, whereas soot showed the opposite seasonal pattern. The source apportionment analysis based on a PMF model constrained by ^{14}C-LHS estimates further revealed pronounced seasonal differences in the sources of BC subfractions. In winter, BB (42.0%) and coal combustion (34.2%) mainly contributed to char, likely reflecting enhanced regional transport from northern China. Traffic-related sources, including gasoline/diesel combustion and road dust, made the largest contributions to char in spring (40.8%) and summer (48.7%), whereas heavy-oil combustion dominated in autumn (42.8%), suggesting a possible influence of coastal and marine shipping emission. In contrast, soot was almost entirely derived from fossil fuel sources, with coal combustion dominating in winter (74.9%) and traffic-related sources prevailing in the other seasons (58.3%-65.4%). These results underscored the effect of regional emission sources and atmospheric transport on the relative abundance of BC subfractions in the background area of the YRD region.

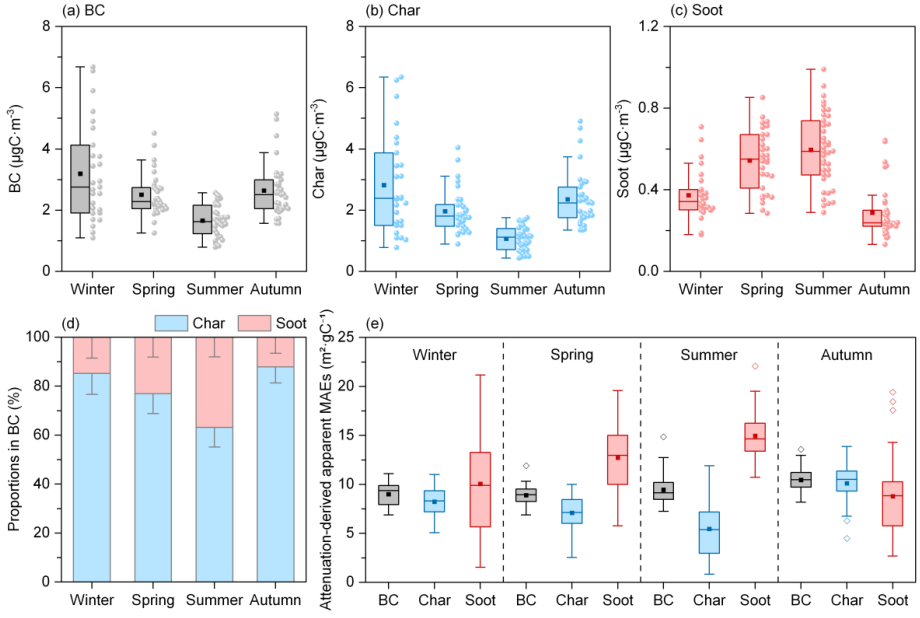
In addition to source contributions, BC subfractions also exhibited distinct attenuation-derived apparent MAE and wet-scavenging responses. Soot showed a higher apparent MAE than char, while MLR-derived source-resolved estimates indicated the highest apparent MAE for fossil-derived soot. Notably, char, particularly from BB sources, was more efficiently removed by precipitation, likely resulting in precipitation-driven fractionation during transport. Consequently, the remaining BC particles in the atmosphere during precipitation events became enriched in fossil-derived components, particularly soot. In contrast, soot concentrations remained statistically unchanged, whereas soot apparent absorption and apparent MAE increased with precipitation amount, likely reflecting

https://doi.org/10.5194/egusphere-2026-6403
Preprint. Discussion started: 10 November 2026
© Author(s) 2026. CC BY 4.0 License.

humidity-related changes in particle mixing state and coating-induced absorption enhancement. These findings elucidated the source-dependent wet removal mechanism of BC from the perspective of its subfraction forms, thereby establishing a linkage between BC sources, char/soot composition, wet removal efficiency, and apparent light absorption properties in a regional background atmosphere.

Furthermore, background or receptor observations are widely employed to constrain BC emission inventories and evaluate model performance. Our results suggest that the source composition of BC at receptor sites may be influenced not only by emissions and transport but also by the selective wet removal of different BC sources and subfractions. In particular, preferential removal of biomass-derived char may alter the relative contributions of fossil and non-fossil BC observed at background sites. Therefore, source- and subfraction-dependent wet scavenging should be considered when interpreting receptor-site BC observations and representing BC atmospheric lifetime, long-range transport, optical properties in models, and source inversion studies.

https://doi.org/10.5194/egusphere-2026-6403
Preprint. Discussion started: 10 November 2026
© Author(s) 2026. CC BY 4.0 License.

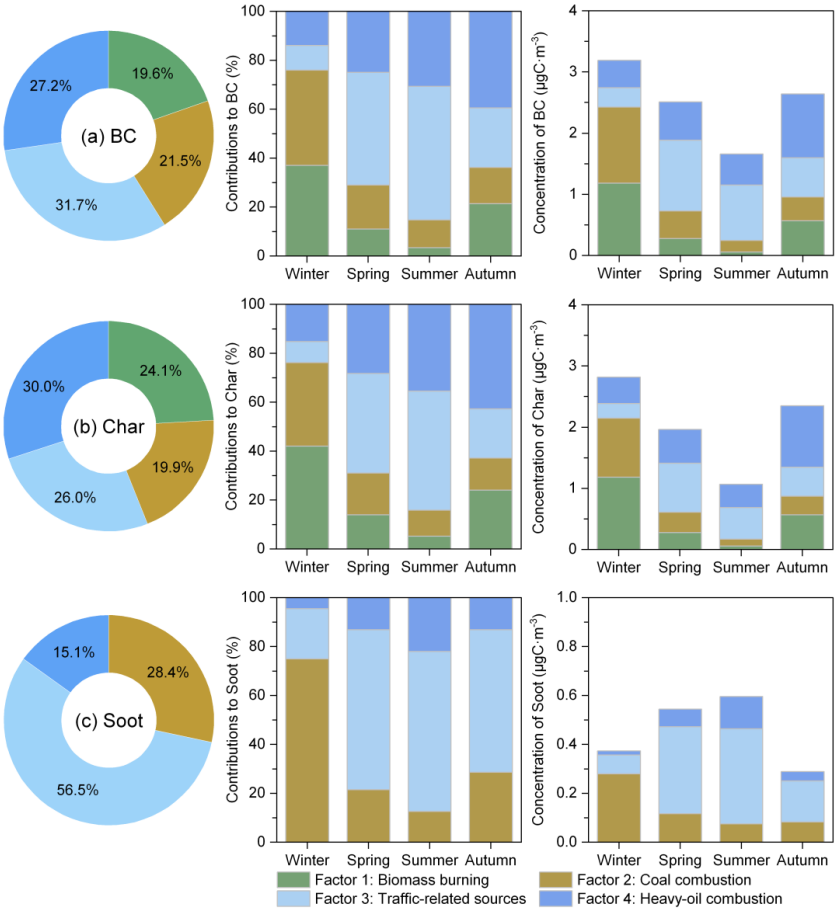


547

548 Figure 1 Seasonal variation of BC, char, soot mass concentrations and their apparent MAE in

549 $PM_{2.5}$ over Lin'an during the observation period.

https://doi.org/10.5194/egusphere-2026-6403
Preprint. Discussion started: 10 November 2026
© Author(s) 2026. CC BY 4.0 License.

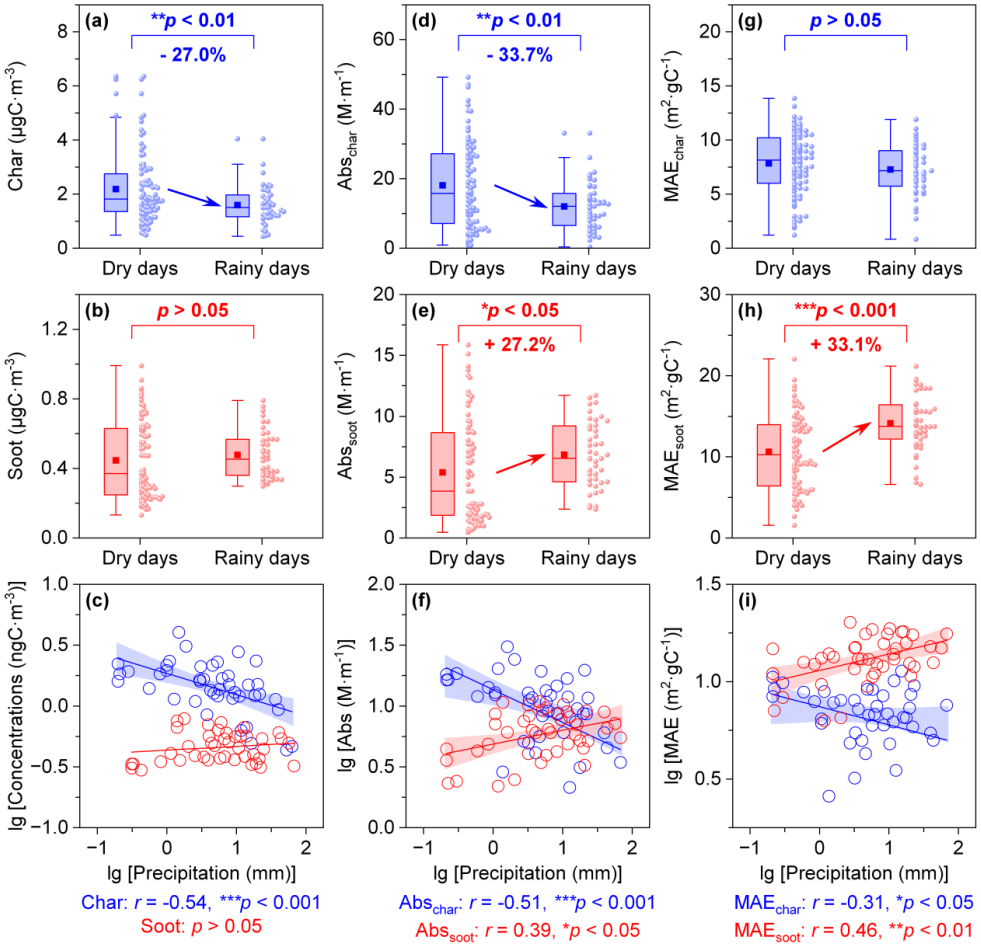


550

551 Figure 2 Seasonal patterns of mass concentrations and contribution fractions of various

552 sources to BC, char, and soot based on ^{14}C-LHS-PMF model.

https://doi.org/10.5194/egusphere-2026-6403
Preprint. Discussion started: 10 November 2026
© Author(s) 2026. CC BY 4.0 License.



553

554 Figure 3 (a-f) Comparisons analysis under rainy versus non-rainy conditions of atmospheric
555 concentrations, apparent absorptions (Abs), and apparent MAE of char and soot. (g-i) Scatter
556 distributions and curves of the linear regression equation between the concentration, apparent
557 absorptions, and apparent MAE of char and soot in $PM_{2.5}$ with precipitation amount at Lin'an
558 during the sampling period. (Significant items, i.e., $p < 0.05$, showed confidence intervals,
559 and confidence intervals were shaded in shadow color.)

https://doi.org/10.5194/egusphere-2026-6403
Preprint. Discussion started: 10 November 2026
© Author(s) 2026. CC BY 4.0 License.

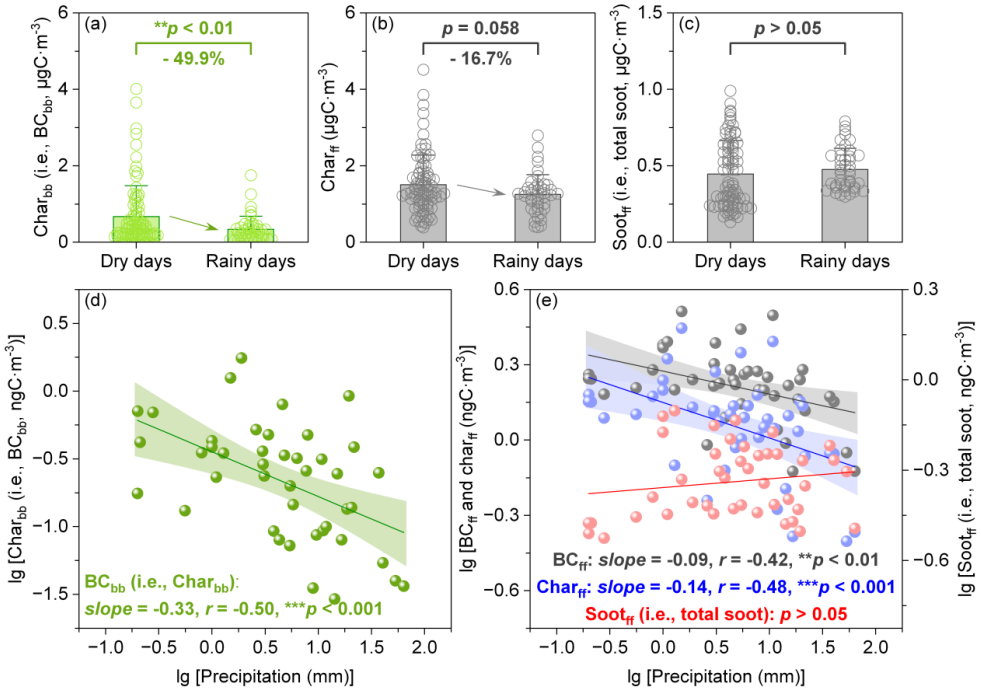


Figure 4 (a-c) Comparisons analysis under rainy versus non-rainy conditions of atmospheric concentrations of char and soot from BB and fossil-fuel-related sources based on ^{14}C-LHS-PMF model. (d-e) The scatter distributions and curves of the linear regression equation between the concentrations of BC_{bb} (i.e., $char_{bb}$), BC_{ff}, $char_{ff}$, and $soot_{ff}$ (i.e., total soot) in $PM_{2.5}$ with precipitation amount at Lin'an during the sampling period. (Significant items, i.e., $p < 0.05$, showed confidence intervals, and confidence intervals were shaded in shadow color.)

https://doi.org/10.5194/egusphere-2026-6403
Preprint. Discussion started: 10 November 2026
© Author(s) 2026. CC BY 4.0 License.

Data availability.

All data used in this study are provided in the paper and Supplementary Materials. Additional data related to this paper can be requested from the corresponding author (caofangle@163.com). The air mass back-trajectory data were acquired from NOAA's Air Resources Laboratory (ftp://arlftp.arlhq.noaa.gov/pub/archives/) [Dataset]. The air mass back-trajectory plotting, Cluster analysis and further image processing were performed by MeteoInfo software (http://www.meteothink.org/downloads/) [Software]. The LHS was performed using MATLAB software (https://www.mathworks.com/) [Software]. The PMF model was performed using EPA PMF 5.0 software (https://www.epa.gov/air-research/) [Software]. Data analysis and figure creation were conducted using Origin 2026 (https://www.originlab.com/) [Software] and Microsoft Office (https://www.microsoft.com/zh-cn/) [Software].

Supplement.

The supplement related to this paper is available online.

Author contributions.

Changliu Wu conducted the primary laboratory experiments, performed the formal data analysis, and wrote the original draft. Fang Cao and Yanlin Zhang conceptualized and designed the research, and provided critical review and editing of the manuscript. Feng Xie, Xiaoying Yang, Wenhuai Song, and Mingyuan Yu contributed to data curation and supplied the measurement datasets. Qianli Ma, Yuan Dai, Xiaofang Jia, and Sönke Szidat provided the

https://doi.org/10.5194/egusphere-2026-6403
Preprint. Discussion started: 10 November 2026
© Author(s) 2026. CC BY 4.0 License.

laboratory facilities and analytical resources.

Competing interests.

The authors declare that they have no conflict of interest.

Acknowledgements.

We sincerely thank all relevant staff members from CAWNET of CMA for aerosol sampling; Chongguo Tian, Zeyu Sun, Rong Sun, and Yuchen Li from Yantai Institute of Coastal Zone Research, Chinese Academy of Sciences for the BC measurement; Yujie Yang, Dan Zhu, Guofeng Tong, Ning Wang, and Houjun Wang from Yangzhou Environmental Monitoring Center for the metal elements measurement.

Financial support.

This research has been supported by the National Natural Science Foundation of China (Grant No. 42192512, 42273087, 41977185) and Scientific Research and Innovation Plan for graduate students in Jiangsu Province (Grant No. KYCX25_1599).

https://doi.org/10.5194/egusphere-2026-6403
Preprint. Discussion started: 10 November 2026
© Author(s) 2026. CC BY 4.0 License.

References

Ammerlaan, B. A. J., Holzinger, R., Jedynska, A. D., and Henzing, J. S.: Technical note: Aerosol light absorption measurements with a carbon analyser-Calibration and precision estimates, Atmospheric Environment, 164, 1-7, https://doi.org/10.1016/j.atmosenv.2017.05.031, 2017.

Blanco-Donado, E. P., Schneider, I. L., Artaxo, P., Lozano-Osorio, J., Portz, L., and Oliveira, M. L.: Source identification and global implications of black carbon, Geoscience Frontiers, 13, 101149, https://doi.org/10.1016/j.gsf.2021.101149, 2022.

Bond, T. C. and Bergstrom, R. W.: Light absorption by carbonaceous particles: An investigative review, Aerosol science and technology, 40, 27-67, https://doi.org/10.1080/02786820500421521, 2006.

Cai, J., Chen, Y., Zeng, J., Jiang, H., Han, Y., Cui, M., Peng, Y., Liu, Z., Zhang, G., and Chen, J.: Physicochemical Properties and Aging Behavior of Black Carbon across Emission Sources Determined by Char and Soot Subgroups, Environmental Science & Technology, 60, 8018-8028, https://doi.org/10.1021/acs.est.5c13279, 2026.

Cai, J., Jiang, H., Chen, Y., Liu, Z., Han, Y., Shen, H., Song, J., Li, J., Zhang, Y., and Wang, R.: Char dominates black carbon aerosol emission and its historic reduction in China, Nature Communications, 14, 6444, https://doi.org/10.1038/s41467-023-42192-8, 2023.

Cao, F., Zhang, Y.-X., Lin, X., and Zhang, Y.-L.: Characteristics and source apportionment of non-polar organic compounds in $PM_{2.5}$ from the three megacities in Yangtze River Delta region, China, Atmospheric Research, 252, 105443, https://doi.org/10.1016/j.atmosres.2020.105443, 2021.

Cao, F., Zhang, Y.-X., Zhang, Y.-L., Song, W.-H., Zhang, Y.-X., Lin, Y.-C., Gul, C., and Haque, M. M.: Molecular compositions of marine organic aerosols over the Bohai and Yellow Seas: Influence of primary emission and secondary formation, Atmospheric Research, 297, 107088, https://doi.org/10.1016/j.atmosres.2023.107088, 2024.

Cao, F., Zhang, Y., Ren, L., Liu, J., Li, J., Zhang, G., Liu, D., Sun, Y., Wang, Z., and Shi, Z.: New insights into the sources and formation of carbonaceous aerosols in China: potential applications of dual-carbon isotopes, National Science Review, 4, 804-806, https://doi.org/10.1093/nsr/nwx097, 2017.

Cao, J., Lee, S., Chow, J. C., Watson, J. G., Ho, K., Zhang, R., Jin, Z., Shen, Z., Chen, G., and Kang, Y.: Spatial and seasonal distributions of carbonaceous aerosols over China, Journal of geophysical research: atmospheres, 112, https://doi.org/10.1029/2006JD008205, 2007.

Cappa, C. D., Onasch, T. B., Massoli, P., Worsnop, D. R., Bates, T. S., Cross, E. S., Davidovits, P., Hakala, J., Hayden, K. L., and Jobson, B. T.: Radiative absorption enhancements due to the mixing state of atmospheric black carbon, Science, 337, 1078-1081, https://doi.org/10.1126/science.1223447, 2012.

Chen, B., Andersson, A., Lee, M., Kirillova, E. N., Xiao, Q., Kruså, M., Shi, M., Hu, K., Lu, Z., and Streets, D. G.: Source forensics of black carbon aerosols from China, Environmental science & technology, 47, 9102-9108, https://doi.org/10.1021/es401599r, 2013.

Chen, L.-W. A., Moosmüller, H., Arnott, W. P., Chow, J. C., Watson, J. G., Susott, R. A., Babbitt, R. E., Wold, C. E., Lincoln, E. N., and Hao, W. M.: Emissions from laboratory combustion of wildland fuels: Emission factors and source profiles, Environmental science & technology, 41, 4317-4325, https://doi.org/10.1021/es062364i, 2007.

Cheng, S., Wang, Y., and An, X.: Temporal variation and source identification of black carbon at Lin'an and Longfengshan regional background stations in China, Journal of Meteorological Research, 31, 1070-1084, https://doi.org/10.1007/s13351-017-7030-5, 2017.

Choi, Y., Kanaya, Y., Takigawa, M., Zhu, C., Park, S.-M., Matsuki, A., Sadanaga, Y., Kim, S.-W., Pan, X., and Pisso, I.: Investigation of the wet removal rate of black carbon in East Asia: Validation of a below-and

https://doi.org/10.5194/egusphere-2026-6403
Preprint. Discussion started: 10 November 2026
© Author(s) 2026. CC BY 4.0 License.

in-cloud wet removal scheme in FLEXPART v10.4, Atmospheric Chemistry and Physics Discussions, 2020, 1-25, https://doi.org/10.5194/acp-20-13655-2020, 2020.

Chow, J. C., Watson, J. G., Kuhns, H., Etyemezian, V., Lowenthal, D. H., Crow, D., Kohl, S. D., Engelbrecht, J. P., and Green, M. C.: Source profiles for industrial, mobile, and area sources in the Big Bend Regional Aerosol Visibility and Observational study, Chemosphere, 54, 185-208, https://doi.org/10.1016/j.chemosphere.2003.07.004, 2004.

Collaud Coen, M., Weingartner, E., Apituley, A., Ceburnis, D., Fierz-Schmidhauser, R., Flentje, H., Henzing, J., Jennings, S. G., Moerman, M., and Petzold, A.: Minimizing light absorption measurement artifacts of the Aethalometer: evaluation of five correction algorithms, Atmospheric Measurement Techniques, 3, 457-474, https://doi.org/10.5194/amt-3-457-2010, 2010.

Coppola, A. I., Wagner, S., Lennartz, S. T., Seidel, M., Ward, N. D., Dittmar, T., Santín, C., and Jones, M. W.: The black carbon cycle and its role in the Earth system, Nature Reviews Earth & Environment, 3, 516-532, https://doi.org/10.1038/s43017-022-00316-6, 2022.

Dasari, S., Andersson, A., Kim, S.-W., Holmstrand, H., Budhavant, K., and Gustafsson, O. r.: Observationally Constrained Wintertime Emission Fluxes and Atmospheric Lifetime of Black Carbon in South Asia, Environmental Science & Technology Letters, 12, 710-717, https://doi.org/10.1021/acs.estlett.5c00079, 2025.

Drinovec, L., Gregorič, A., Zotter, P., Wolf, R., Bruns, E. A., Prévôt, A. S. H., Petit, J.-E., Favez, O., Sciare, J., Arnold, I. J., Chakrabarty, R. K., Moosmüller, H., Filep, A., and Močnik, G.: The filter-loading effect by ambient aerosols in filter absorption photometers depends on the coating of the sampled particles, Atmospheric Measurement Techniques, 10, 1043-1059, https://doi.org/10.5194/amt-10-1043-2017, 2017.

Du, W., Ding, Z., Lei, Y., Zhang, S., Wu, C., Zhang, F., Wang, F., Lv, S., Liu, X., and Meng, J.: Atmospheric fine particulate dicarboxylic acids and related SOA in winter at the background site of Yangtze River Delta: Implication for the long-distance transport of solid fuels burning, Atmospheric Environment, 289, 119320, https://doi.org/10.1016/j.atmosenv.2022.119320, 2022.

Fan, M.-Y., Zhang, Y.-L., Lin, Y.-C., Li, J., Cheng, H., An, N., Sun, Y., Qiu, Y., Cao, F., and Fu, P.: Roles of sulfur oxidation pathways in the variability in stable sulfur isotopic composition of sulfate aerosols at an urban site in Beijing, China, Environmental Science & Technology Letters, 7, 883-888, https://doi.org/10.1021/acs.estlett.0c00623, 2020.

Feng, X., Chen, Y., Jiang, H., Cai, J., Liu, Z., Feng, Y., Li, M., Mu, Y., Chen, J., and Chen, T.: Combination of multiple isotopes and PMF model provide insights into the method optimization of $PM_{2.5}$ source apportionment during haze episodes, Journal of Geophysical Research: Atmospheres, 129, e2024JD041350, https://doi.org/10.1029/2024JD041350, 2024.

Fierce, L., Bond, T. C., Bauer, S. E., Mena, F., and Riemer, N.: Black carbon absorption at the global scale is affected by particle-scale diversity in composition, Nature communications, 7, 12361, https://doi.org/10.1038/ncomms12361, 2016.

Fu, Y., Peng, X., Guo, Z., Peng, L., Lin, Q., Li, L., Li, M., Chen, D., Zhang, G., and Bi, X.: Filter-based absorption enhancement measurement for internally mixed black carbon particles over southern China, Science of The Total Environment, 762, 144194, https://doi.org/10.1016/j.scitotenv.2020.144194, 2021.

Gelencsér, A., May, B., Simpson, D., Sánchez-Ochoa, A., Kasper-Giebl, A., Puxbaum, H., Caseiro, A., Pio, C., and Legrand, M.: Source apportionment of $PM_{2.5}$ organic aerosol over Europe: Primary/secondary, natural/anthropogenic, and fossil/biogenic origin, Journal of Geophysical Research: Atmospheres, 112, https://doi.org/10.1029/2006JD008094, 2007.

Geng, X., Li, J., Zhong, G., Zhao, S., Tian, C., Zhang, Y.-L., and Zhang, G.: Ship Emissions as the Largest

https://doi.org/10.5194/egusphere-2026-6403
Preprint. Discussion started: 10 November 2026
© Author(s) 2026. CC BY 4.0 License.

Contributor to Coastal Atmospheric Black Carbon at a Receptor Island in Southern China, Environmental Science & Technology Letters, https://doi.org/10.1021/acs.estlett.4c00362, 2024.

Han, Y., Cao, J., Lee, S., Ho, K., and An, Z.: Different characteristics of char and soot in the atmosphere and their ratio as an indicator for source identification in Xi'an, China, Atmospheric Chemistry and Physics, 10, 595-607, https://doi.org/10.5194/acp-10-595-2010, 2010.

Han, Y., Lee, S., Cao, J., Ho, K., and An, Z.: Spatial distribution and seasonal variation of char-EC and soot-EC in the atmosphere over China, Atmospheric Environment, 43, 6066-6073, https://doi.org/10.1016/j.atmosenv.2009.08.018, 2009.

Han, Y., Chen, Y., Feng, Y., Shang, Y., Li, J., Li, Q., and Chen, J.: Existence and formation pathways of high-and low-maturity elemental carbon from solid fuel combustion by a time-resolved study, Environmental Science & Technology, 56, 2551-2561, https://doi.org/10.1021/acs.est.1c05216, 2022.

Han, Y., Cao, J., Chow, J. C., Watson, J. G., An, Z., Jin, Z., Fung, K., and Liu, S.: Evaluation of the thermal/optical reflectance method for discrimination between char-and soot-EC, Chemosphere, 69, 569-574, https://doi.org/10.1016/j.chemosphere.2007.03.024, 2007.

Han, Y., Han, Z., Cao, J., Chow, J., Watson, J., An, Z., Liu, S., and Zhang, R.: Distribution and origin of carbonaceous aerosol over a rural high-mountain lake area, Northern China and its transport significance, Atmospheric Environment, 42, 2405-2414, https://doi.org/10.1016/j.atmosenv.2007.12.020, 2008.

Han, Y., Chen, Y., Ahmad, S., Feng, Y., Zhang, F., Song, W., Cao, F., Zhang, Y., Yang, X., and Li, J.: High time-and size-resolved measurements of PM and chemical composition from coal combustion: implications for the EC formation process, Environmental science & technology, 52, 6676-6685, https://doi.org/10.1021/acs.est.7b05786, 2018.

Huang, L., Gong, S., Jia, C., and Lavoué, D.: Importance of deposition processes in simulating the seasonality of the Arctic black carbon aerosol, Journal of Geophysical Research: Atmospheres, 115, https://doi.org/10.1029/2009JD013478, 2010.

Huang, R.-J., Zhang, Y., Bozzetti, C., Ho, K.-F., Cao, J.-J., Han, Y., Daellenbach, K. R., Slowik, J. G., Platt, S. M., and Canonaco, F.: High secondary aerosol contribution to particulate pollution during haze events in China, Nature, 514, 218-222, https://doi.org/10.1038/nature13774, 2014.

Li, C., Hu, Z., Kang, S., Kirillova, E. N., Yan, F., Chen, P., Shen, G., Jake, T. T., and Gustafsson, Ö.: Longer Lifetime of BC from Fossil Fuel Combustion than from Biomass Burning: $\Delta^{14}C$ Evidence, Environmental Science & Technology, 10.1021/acs.est.4c10040, https://doi.org/10.1021/acs.est.4c10040, 2025.

Li, W., Riemer, N., Xu, L., Wang, Y., Adachi, K., Shi, Z., Zhang, D., Zheng, Z., and Laskin, A.: Microphysical properties of atmospheric soot and organic particles: measurements, modeling, and impacts, npj Climate and Atmospheric Science, 7, 65, https://doi.org/10.1038/s41612-024-00610-8, 2024.

Li, Y., Fu, T.-M., Yu, J. Z., Feng, X., Zhang, L., Chen, J., Boreddy, S. K. R., Kawamura, K., Fu, P., and Yang, X.: Impacts of chemical degradation on the global budget of atmospheric levoglucosan and its use as a biomass burning tracer, Environmental Science & Technology, 55, 5525-5536, https://doi.org/10.1021/acs.est.0c07313, 2021.

Liang, C.-S., Duan, F.-K., He, K.-B., and Ma, Y.-L.: Review on recent progress in observations, source identifications and countermeasures of $PM_{2.5}$, Environment International, 86, 150-170, https://doi.org/10.1016/j.envint.2015.10.016, 2016.

Liang, L., Engling, G., Cheng, Y., Liu, X., Du, Z., Ma, Q., Zhang, X., Sun, J., Xu, W., and Liu, C.: Biomass burning impacts on ambient aerosol at a background site in East China: Insights from a yearlong study, Atmospheric Research, 231, 104660, https://doi.org/10.1016/j.atmosres.2019.104660, 2020.

Lin, Y.-C., Yu, M., Xie, F., and Zhang, Y.: Anthropogenic emission sources of sulfate aerosols in Hangzhou, East

https://doi.org/10.5194/egusphere-2026-6403
Preprint. Discussion started: 10 November 2026
© Author(s) 2026. CC BY 4.0 License.

China: Insights from isotope techniques with consideration of fractionation effects between gas-to-particle transformations, Environmental Science & Technology, 56, 3905-3914, https://doi.org/10.1021/acs.est.1c05823, 2022.

Lin, Y.-C., Zhang, Y.-L., Song, W., Yang, X., and Fan, M.-Y.: Specific sources of health risks caused by size-resolved PM-bound metals in a typical coal-burning city of northern China during the winter haze event, Science of the Total Environment, 734, 138651, https://doi.org/10.1016/j.scitotenv.2020.138651, 2020.

Liu, D., Whitehead, J., Alfarra, M. R., Reyes-Villegas, E., Spracklen, D. V., Reddington, C. L., Kong, S., Williams, P. I., Ting, Y.-C., and Haslett, S.: Black-carbon absorption enhancement in the atmosphere determined by particle mixing state, Nature Geoscience, 10, 184-188, https://doi.org/10.1038/ngeo2901, 2017.

Liu, H., Wang, Q., Qu, Y., Tian, J., Li, L., Ma, N., Zhou, Y., Ran, W., Su, H., and Han, Y.: High contributions of fossil fuel sources to char-EC/soot-EC at a high-altitude site: Direct radiative effects and transport pathway, Fuel, 361, 130632, https://doi.org/10.1016/j.fuel.2023.130632, 2024.

Liu, H., Wang, Q., Tian, J., Wang, J., Tian, R., Zhang, Y., Zhang, Q., Xue, Y., Xu, H., and Ran, W.: Source-specific mass absorption efficiencies of char-EC and soot-EC improve accuracy in black carbon radiative effect estimation, Journal of Geophysical Research: Atmospheres, 130, e2024JD043079, https://doi.org/10.1029/2024JD043079, 2025a.

Liu, J., Jiang, F., Wang, Q., Zhang, G., Li, J., Chen, W., Ding, P., Zhu, S., Cheng, Z., and Zhang, X.: Substantial reductions in black carbon from both fossil fuels and biomass burning during China's Clean Air Action, Proceedings of the National Academy of Sciences, 122, e2500843122, https://doi.org/10.1073/pnas.2500843122, 2025b.

Lohmann, U., Friebel, F., Kanji, Z. A., Mahrt, F., Mensah, A. A., and Neubauer, D.: Future warming exacerbated by aged-soot effect on cloud formation, Nature Geoscience, 13, 674-680, https://doi.org/10.1038/s41561-020-0631-0, 2020.

Niu, Z., Wang, S., Chen, J., Zhang, F., Chen, X., He, C., Lin, L., Yin, L., and Xu, L.: Source contributions to carbonaceous species in PM2. 5 and their uncertainty analysis at typical urban, peri-urban and background sites in southeast China, Environmental pollution, 181, 107-114, https://doi.org/10.1016/j.envpol.2013.06.006, 2013.

Ram, K. and Sarin, M.: Absorption coefficient and site-specific mass absorption efficiency of elemental carbon in aerosols over urban, rural, and high-altitude sites in India, Environmental science & technology, 43, 8233-8239, https://doi.org/10.1021/es9011542, 2009.

Ren, Y., Wang, G., Tao, J., Zhang, Z., Wu, C., Wang, J., Li, J., Wei, J., Li, H., and Meng, F.: Seasonal characteristics of biogenic secondary organic aerosols at Mt. Wuyi in Southeastern China: Influence of anthropogenic pollutants, Environmental pollution, 252, 493-500, https://doi.org/10.1016/j.envpol.2019.05.077, 2019.

Réveillet, M., Dumont, M., Gascoin, S., Lafaysse, M., Nabat, P., Ribes, A., Nheili, R., Tuzet, F., Ménégoz, M., and Morin, S.: Black carbon and dust alter the response of mountain snow cover under climate change, Nature communications, 13, 5279, https://doi.org/10.1038/s41467-022-32501-y, 2022.

Rodríguez, B., Huang, L., Santos, G., Zhang, W., Vetro, V., Xu, X., Kim, S., and Czimczik, C.: Seasonal cycle of isotope-based source apportionment of elemental carbon in airborne particulate matter and snow at Alert, Canada, Journal of Geophysical Research: Atmospheres, 125, e2020JD033125, https://doi.org/10.1029/2020JD033125, 2020.

Sharma, S., Ishizawa, M., Chan, D., Lavoué, D., Andrews, E., Eleftheriadis, K., and Maksyutov, S.: 16-year

https://doi.org/10.5194/egusphere-2026-6403
Preprint. Discussion started: 10 November 2026
© Author(s) 2026. CC BY 4.0 License.

simulation of Arctic black carbon: Transport, source contribution, and sensitivity analysis on deposition, Journal of Geophysical Research: Atmospheres, 118, 943-964, https://doi.org/10.1029/2012JD017774, 2013.

Song, W., Zhang, Y., Gao, M., Xie, F., Cao, F., Rauber, M., Kawichai, S., Prapamontol, T., Szidat, S., Peng, Y., Carmichael, G. R., and Zhang, Y.-L.: Biomass burning increase in Southeast Asia is dominated by char black carbon, Communications Earth & Environment, 7, 359, 10.1038/s43247-026-03431-0, https://doi.org/10.1038/s43247-026-03431-0, 2026.

Szidat, S., Salazar, G. A., Vogel, E., Battaglia, M., Wacker, L., Synal, H.-A., and Türler, A.: ^{14}C analysis and sample preparation at the new Bern Laboratory for the Analysis of Radiocarbon with AMS (LARA), Radiocarbon, 56, 561-566, https://doi.org/10.2458/56.17457, 2014.

Szidat, S., Jenk, T. M., Synal, H. A., Kalberer, M., Wacker, L., Hajdas, I., Kasper-Giebl, A., and Baltensperger, U.: Contributions of fossil fuel, biomass-burning, and biogenic emissions to carbonaceous aerosols in Zurich as traced by ^{14}C, Journal of Geophysical Research: Atmospheres, 111, https://doi.org/10.1029/2005JD006590, 2006.

Szidat, S., Ruff, M., Perron, N., Wacker, L., Synal, H.-A., Hallquist, M., Shannigrahi, A. S., Yttri, K. E., Dye, C., and Simpson, D.: Fossil and non-fossil sources of organic carbon (OC) and elemental carbon (EC) in Göteborg, Sweden, Atmospheric Chemistry and Physics, 9, 1521-1535, https://doi.org/10.5194/acp-9-1521-2009, 2009.

Wang, J., Zhang, Q., Chen, M., Collier, S., Zhou, S., Ge, X., Xu, J., Shi, J., Xie, C., and Hu, J.: First chemical characterization of refractory black carbon aerosols and associated coatings over the Tibetan Plateau (4730 m asl), Environmental science & technology, 51, 14072-14082, https://doi.org/10.1021/acs.est.7b03973, 2017a.

Wang, X., Zong, Z., Tian, C., Chen, Y., Luo, C., Li, J., Zhang, G., and Luo, Y.: Combining positive matrix factorization and radiocarbon measurements for source apportionment of $PM_{2.5}$ from a national background site in North China, Scientific reports, 7, 10648, https://doi.org/10.1038/s41598-017-10762-8, 2017b.

Wang, Y., Ju, Q., Xing, Z., Zhao, J., Guo, S., Li, F., and Du, K.: Observation of black carbon in Northern China in winter of 2018-2020 and its implications for black carbon mitigation, Science of The Total Environment, 877, 162897, https://doi.org/10.1016/j.scitotenv.2023.162897, 2023.

Wang, Z., Srivastava, D., Alam, M. S., Crilley, L. R., Kramer, L. J., Rooney, D. J., Saksakulkrai, S., Khare, M., Ascough, P., and Bompard, N.: Dominant contribution of fossil fuel combustion to carbonaceous aerosol pollution in Delhi: Insights from radiocarbon and organic tracers, Journal of Hazardous Materials, 504, 141289, https://doi.org/10.1016/j.jhazmat.2026.141289, 2026.

Wu, B., Xuan, K., Zhang, X., Shen, X., Li, X., Zhou, Q., Cao, X., Zhang, H., and Yao, Z.: Mass absorption cross-section of black carbon from residential biofuel stoves and diesel trucks based on real-world measurements, Science of the Total Environment, 784, 147225, https://doi.org/10.1016/j.scitotenv.2021.147225, 2021.

Wu, C., Cao, F., Zhang, Y., Song, W., Ma, Q., Jia, X., Ren, L., Yang, X., Yu, M., and Szidat, S. n.: Source Apportionment of Organic Aerosol Using ^{14}C and Organic Molecular Tracers at a Regional Background Site of the Yangtze River Delta Region, China, Journal of Geophysical Research: Atmospheres, 130, e2024JD043296, https://doi.org/10.1029/2024JD043296, 2025.

Wu, X., Cao, F., Haque, M., Fan, M.-Y., Zhang, S.-C., and Zhang, Y.-L.: Molecular composition and source apportionment of fine organic aerosols in Northeast China, Atmospheric Environment, 239, 117722, https://doi.org/10.1016/j.atmosenv.2020.117722, 2020.

Xie, F., Cao, F., Popovicheva, O., Huang, Z.-L., Chichaeva, M., Lin, Y.-C., Song, W.-H., Kovach, R.,

https://doi.org/10.5194/egusphere-2026-6403
Preprint. Discussion started: 10 November 2026
© Author(s) 2026. CC BY 4.0 License.

Zavgorodnyaya, Y., and Wu, C.-L.: Wildfires significantly enhance light absorption of black carbon and brown carbon aerosols in Moscow urban atmosphere, Sustainable Horizons, 17, 100169, https://doi.org/10.1016/j.horiz.2025.100169, 2026.

Xing, J.: Sources and atmospheric processes of atmospheric $PM_{2.5}$ in the Yangtze River Estuary based on experimental component analysis and PMF model (Chinese), Master's dissertation, Shang Hai: East China Normal University, https://link.cnki.net/doi/10.27149/d.cnki.ghdsu.2022.004027, 2022.

Xu, H., Cai, J., Feng, X., Jiang, H., Peng, Y., Lu, Y., and Chen, Y.: Chemical and optical distinctions between elemental carbon subcategories Char-EC and Soot-EC: Insights from a haze event in North China, Environmental Pollution, 375, 126306, https://doi.org/10.1016/j.envpol.2025.126306, 2025.

Yan, C., Zheng, M., Shen, G., Cheng, Y., Ma, S., Sun, J., Cui, M., Zhang, F., Han, Y., and Chen, Y.: Characterization of carbon fractions in carbonaceous aerosols from typical fossil fuel combustion sources, Fuel, 254, 115620, https://doi.org/10.1016/j.fuel.2019.115620, 2019.

Yang, X. Y., Cao, F., Lin, Y. C., Fan, M. Y., Wu, C. L., Yu, M. Y., Song, W. H., and Zhang, Y. L.: Distinct sources of char and soot black carbon aerosols during winter haze at pair sites in north China: Source apportionment from dual-carbon isotope constrained PMF, Journal of Geophysical Research: Atmospheres, 130, e2024JD043077, https://doi.org/10.1029/2024JD043077, 2025.

Yttri, K. E., Simpson, D., Stenström, K., Puxbaum, H., and Svendby, T.: Source apportionment of the carbonaceous aerosol in Norway-quantitative estimates based on ^{14}C, thermal-optical and organic tracer analysis, Atmospheric Chemistry and Physics, 11, 9375-9394, https://doi.org/10.5194/acp-11-9375-2011, 2011.

Yttri, K. E., Bäcklund, A., Conen, F., Eckhardt, S., Evangeliou, N., Fiebig, M., Kasper-Giebl, A., Gold, A., Gundersen, H., and Myhre, C. L.: Composition and sources of carbonaceous aerosol in the European Arctic at Zeppelin Observatory, Svalbard (2017 to 2020), Atmospheric Chemistry and Physics, 24, 2731-2758, https://doi.org/10.5194/acp-24-2731-2024, 2024.

Yu, M., Ding, J., Lin, Y.-C., and Zhang, Y.-L.: Divergent Responses to Wet Scavenging: Fossil Fuel Black Carbon Exhibits Longer Lifetime and Stronger Light Absorption than Biomass Burning BC, Environmental Science & Technology Letters, 13, 386-392, https://doi.org/10.1021/acs.estlett.6c00058, 2026.

Yu, M., Lin, Y.-C., Xie, F., Cao, F., and Zhang, Y.-L.: Contrasting char-EC and soot-EC in sources, atmospheric processing, and light-absorbing capabilities: Insights from high-resolution stable carbon isotope analysis, Atmospheric Research, 108275, https://doi.org/10.1016/j.atmosres.2025.108275, 2025.

Yu, M., Zhang, Y.-L., Xie, T., Song, W., Lin, Y.-C., Zhang, Y., Cao, F., Yang, C., and Szidat, S.: Quantification of fossil and non-fossil sources to the reduction of carbonaceous aerosols in the Yangtze River Delta, China: Insights from radiocarbon analysis during 2014-2019, Atmospheric environment, 292, 119421, https://doi.org/10.1016/j.atmosenv.2022.119421, 2023.

Zeng, L., Tan, T., Zhao, G., Du, Z., Hu, S., Shang, D., and Hu, M.: Overestimation of black carbon light absorption due to mixing state heterogeneity, npj Climate and Atmospheric Science, 7, 2, https://doi.org/10.1038/s41612-023-00535-8, 2024.

Zhang, G., Liu, J., Li, J., Li, P., Wei, N., and Xu, B.: Radiocarbon isotope technique as a powerful tool in tracking anthropogenic emissions of carbonaceous air pollutants and greenhouse gases: A review, Fundamental Research, 1, 306-316, https://doi.org/10.1016/j.fmre.2021.03.007, 2021a.

Zhang, L., Luo, Z., Xiong, R., Liu, X., Li, Y., Du, W., Chen, Y., Pan, B., Cheng, H., and Shen, G.: Mass absorption efficiency of black carbon from residential solid fuel combustion and its association with carbonaceous fractions, Environmental Science & Technology, 55, 10662-10671, https://doi.org/10.1021/acs.est.1c02689, 2021b.

https://doi.org/10.5194/egusphere-2026-6403
Preprint. Discussion started: 10 November 2026
© Author(s) 2026. CC BY 4.0 License.

Zhang, X., Wang, J., Wang, Y., Liu, H., Sun, J., and Zhang, Y.: Changes in chemical components of aerosol particles in different haze regions in China from 2006 to 2013 and contribution of meteorological factors, Atmospheric Chemistry and Physics, 15, 12935-12952, https://doi.org/10.5194/acp-15-12935-2015, 2015a.

Zhang, X. Y., Wang, Y. Q., Niu, T., Zhang, X. C., Gong, S. L., Zhang, Y. M., and Sun, J. Y.: Atmospheric aerosol compositions in China: spatial/temporal variability, chemical signature, regional haze distribution and comparisons with global aerosols, Atmospheric Chemistry and Physics, 12, 779-799, https://doi.org/10.5194/acp-12-779-2012, 2012.

Zhang, Y.-L., Cerqueira, M., Salazar, G., Zotter, P., Hueglin, C., Zellweger, C., Pio, C., Prévôt, A. S., and Szidat, S.: Wet deposition of fossil and non-fossil derived particulate carbon: Insights from radiocarbon measurement, Atmospheric environment, 115, 257-262, https://doi.org/10.1016/j.atmosenv.2015.06.005, 2015b.

Zhang, Y.-L., Huang, R.-J., El Haddad, I., Ho, K.-F., Cao, J.-J., Han, Y., Zotter, P., Bozzetti, C., Daellenbach, K., and Canonaco, F.: Fossil vs. non-fossil sources of fine carbonaceous aerosols in four Chinese cities during the extreme winter haze episode of 2013, Atmospheric Chemistry and Physics, 15, 1299-1312, https://doi.org/10.5194/acp-15-1299-2015, 2015c.

Zhang, Y.-L., Schnelle-Kreis, J. r., Abbaszade, G. l., Zimmermann, R., Zotter, P., Shen, R.-r., Schäfer, K., Shao, L., Prévôt, A. S., and Szidat, S. n.: Source apportionment of elemental carbon in Beijing, China: insights from radiocarbon and organic marker measurements, Environmental science & technology, 49, 8408-8415, https://doi.org/10.1021/acs.est.5b01944, 2015d.

Zhang, Y., Liu, D., Shen, C., Ding, P., and Zhang, G.: Development of a preparation system for the radiocarbon analysis of organic carbon in carbonaceous aerosols in China, Nuclear Instruments and Methods in Physics Research Section B: Beam Interactions with Materials and Atoms, 268, 2831-2834, https://doi.org/10.1016/j.nimb.2010.06.032, 2010.

Zhang, Y., Cao, F., Song, W., Jia, X.-F., Xie, T., Wu, C.-L., Yan, P., Yu, M., Rauber, M., and Salazar, G.: Fossil and Nonfossil Sources of Winter Organic Aerosols in the Regional Background Atmosphere of China, Environmental science & technology, 58, 1244-1254, https://doi.org/10.1021/acs.est.3c08491, 2024.

Zhang, Y., Favez, O., Canonaco, F., Liu, D., Močnik, G., Amodeo, T., Sciare, J., Prévôt, A. S., Gros, V., and Albinet, A.: Evidence of major secondary organic aerosol contribution to lensing effect black carbon absorption enhancement, npj climate and atmospheric science, 1, 47, https://doi.org/10.1038/s41612-018-0056-2, 2018.

Zhang, Y., Zhang, X., Zhong, J., Sun, J., Shen, X., Zhang, Z., Xu, W., Wang, Y., Liang, L., and Liu, Y.: On the fossil and non-fossil fuel sources of carbonaceous aerosol with radiocarbon and AMS-PMF methods during winter hazy days in a rural area of North China plain, Environmental Research, 208, 112672, https://doi.org/10.1016/j.envres.2021.112672, 2022.

Zhang, Z., Zhou, L., and Zhang, M.: A numerical sensitivity study on the snow-darkening effect by black carbon deposition over the Arctic in spring, Atmospheric Chemistry and Physics, 25, 1-25, https://doi.org/10.5194/acp-25-1-2025, 2025a.

Zhang, Z., Wang, Y., Chen, X., Xu, L., Zheng, Z., Ching, J., Zhu, S., Liu, D., and Li, W.: Absorption enhancement and shielding effect of brown organic coating on black carbon aerosols, npj Climate and Atmospheric Science, 8, 102, https://doi.org/10.1038/s41612-025-00989-y, 2025b.

Zhao, H., Niu, Z., Zhou, W., Wang, S., Feng, X., Wu, S., Lu, X., and Du, H.: Measurement report: Source apportionment of carbonaceous aerosol using dual-carbon isotopes (^{13}C and ^{14}C) and levoglucosan in three northern Chinese cities during 2018-2019, Atmospheric Chemistry and Physics, 22, 6255-6274, https://doi.org/10.5194/acp-22-6255-2022, 2022.

https://doi.org/10.5194/egusphere-2026-6403
Preprint. Discussion started: 10 November 2026
© Author(s) 2026. CC BY 4.0 License.



Zheng, H., Kong, S., Chen, N., Fan, Z., Zhang, Y., Yao, L., Cheng, Y., Zheng, S., Yan, Y., and Liu, D.: A method to dynamically constrain black carbon aerosol sources with online monitored potassium, npj Climate and Atmospheric Science, 4, 43, https://doi.org/10.1038/s41612-021-00200-y, 2021.

Zheng, M., Yan, C., Wang, S., He, K., and Zhang, Y.: Understanding PM2. 5 sources in China: challenges and perspectives, National Science Review, 4, 801-803, https://doi.org/10.1093/nsr/nwx129, 2017.

Zhi, G., Chen, Y., Sun, J., Chen, L., Tian, W., Duan, J., Zhang, G., Chai, F., Sheng, G., and Fu, J.: Harmonizing aerosol carbon measurements between two conventional thermal/optical analysis methods, Environmental science & technology, 45, 2902-2908, https://doi.org/10.1021/es102803f, 2011.

Zhu, C., Kanaya, Y., Takigawa, M., Ikeda, K., Tanimoto, H., Taketani, F., Miyakawa, T., Kobayashi, H., and Pisso, I.: FLEXPART v10.1 simulation of source contributions to Arctic black carbon, Atmospheric Chemistry and Physics, 20, 1641-1656, https://doi.org/10.5194/acp-20-1641-2020, 2020.

Zong, Z., Wang, X., Tian, C., Chen, Y., Fu, S., Qu, L., Ji, L., Li, J., and Zhang, G.: PMF and PSCF based source apportionment of $PM_{2.5}$ at a regional background site in North China, Atmospheric research, 203, 207-215, https://doi.org/10.1016/j.atmosres.2017.12.013, 2018.

Zong, Z., Wang, X., Tian, C., Chen, Y., Qu, L., Ji, L., Zhi, G., Li, J., and Zhang, G.: Source apportionment of $PM_{2.5}$ at a regional background site in North China using PMF linked with radiocarbon analysis: insight into the contribution of biomass burning, Atmospheric Chemistry and Physics, 16, 11249-11265, https://doi.org/10.5194/acp-16-11249-2016, 2016.